Morphology, ultrastructure, and phylogeny of two novel species of *Ventrifissura* (*V. oblonga* n. sp. and *V. velata* n. sp., Thecofilosea, Cercozoa)

Takashi Shiratori[a,b,1], Yabuki Akinori[b], Ken-ichiro Ishida[a]

[a]Faculty of Life and Environmental Sciences, University of Tsukuba, Tsukuba, Ibaraki 305-8572, Japan

[b]Japan Agency for Marine-Earth Science and Technology (JAMSTEC), 2-15 Natsushima, Yokosuka, Kanagawa, 237-0061, Japan

[1]Corresponding Author

T. Shiratori, Japan Agency for Marine-Earth Science and Technology (JAMSTEC), 2-15 Natsushima, Yokosuka, Kanagawa 237-0061, Japan

Telephone number: +81-46867-9524

FAX number: +81-46867-9525;

e-mail: tshiratori@jamstec.go.jp

wb.takashi@gmail.com

Running title: Description of two novel *Ventrifissura* species

Declarations of interest: none

Abstract

Ventrifissura is a group of poorly studied heterotrophic biflagellates in the phylum Cercozoa. Despite a phylogenetic placement with only weak support and a lack of ultrastructural data, *Ventrifissura* was assigned to Thecofilosea. In the presented study, we established cultures of two novel species of *Ventrifissura* (*V*. *oblonga* n. sp. and *V*. *velata* n. sp.) isolated from coastal marine environments in Japan, and performed light and electron microscopy observations and molecular phylogenetic analysis. Transmission electron microscopy revealed that *V*. *oblonga* shares several ultrastructural characteristics with thecofilosean flagellates, including permanently condensed chromosomes, a extracellular theca, and slender extrusomes. Molecular phylogenetic analysis could not resolve the phylogenetic position, but the possibility that *Ventrifissura* clusters into Ventrifilosa was supported by approximately unbiased tests. Based on both morphological and phylogenetic findings, we concluded that *Ventrifissura* is a basal lineage of Thecofilosea.

Keywords: Morphology, ultrastructure, phylogeny, *Ventrifissura*, Cercozoa, Thecofilosea

Introduction

Thecofilosea is one of cercozoan classes that was established based on molecular phylogenetic analysis using small subunit ribosomal RNA (SSU rRNA) gene sequences (Cavalier-Smith and Chao 2003). This group originally comprised thecate amoebae (Tectofilosida) and amoeboflagellates (*Cryothecomonas*) and was defined as a protistan group in which individuals possess an organic flexible theca or rigid test (Cavalier-Smith and Chao 2003). Further molecular phylogenetic analyses have revealed that protists with uncertain taxonomic positions exemplified by *Ebria* and *Protaspa*, and protists that have been classified into other taxonomic groups such as phaeodareans also belong to

Thecofilosea (Hoppenrath and Leander 2006a, b; Yuasa et al. 2006). Thecofilosean protists such as *Mataza*, *Botuliforma*, *Ventrifissura*, and *Verrucomonas* have also been described recently (Chantangsi and Leander 2010a; Yabuki and Ishida 2011), and Thecofilosea currently consists of seven orders (Cavalier-Smith et al. 2018). Diversity of thecofilosean thecate amoebae also have been revealed recently (Dumack et al. 2017; 2018). However, some newly assigned thecofiloseans lack sufficient morphological and ultrastructural information, which prevents a deep understanding of the evolution of Thecofilosea.

The genus *Ventrifissura* is a group of marine heterotrophic biflagellates first reported by Chantangsi and Leander (2010a). Two species (*V. artocarpoidea* and *V. foliiformis*) isolated from tidal sand flats in British Columbia, Canada, were originally reported and characterized based on culture-independent light microscopy and molecular phylogenetic analysis using SSU rRNA gene sequences. Cells are broadly obovate and dorsoventrally flattened, and they move by gliding across a substrate. Cells have a longitudinal groove at the ventral side and a large nucleus at the anterior region. The cell surface of *V. foliiformis* is smooth, whereas that of *V. artocarpoidea* is decorated with numerous pointed warts. Although Chantangsi and Leander (2010a) assigned *Ventrifissura* as a member of Tectofilosida based on molecular phylogenetic analysis, a subsequent taxon-rich SSU rRNA gene tree showed that *Ventrifissura* is positioned as the deepest lineage of Thecofilosea, together with a group of uncultured heterotrophic flagellates *Verrucomonas*, albeit with weak statistical support (Howe et al. 2011). *Ventrifissura* and *Verrucomonas* share several morphological features with some thecofilosean flagellates (e.g., *Protaspa* and *Cryothecomonas*) based on light microscopy, such as a non-flexible cell body and ventral groove. Based on phylogenetic position and morphological similarity, the two genera were classified into the new thecofilosean order Ventricleftida (Howe et al. 2011). However, *Ventrifissura* lacks ultrastructural information that is important for higher classification of

Cercozoa. In addition, the monophyly of *Ventrifissura* and Thecofilosea was not consistently supported in molecular phylogenetic analyses, and *Ventrifissura* occasionally branches as a sister or inner lineage of Imbricatea (Chantangsi and Leander 2010b; Dumack et al. 2017; Scoble and Cavalier-Smith 2014).

In the present study, we established cultures of two new species of *Ventrifissura* from Japanese coastal marine samples, and performed molecular phylogenetic analysis and light and electron microscopic observations. Our results provide insight on the taxonomic position of *Ventrifissura* and ultrastructural evolution of Thecofilosea.

Results

Light microscopy analysis of *V. oblonga* and *V. velata*

Ventrifissura oblonga had a rigid cell body and smooth cell surface (Fig. 1). Cells were ovoid in shape and slightly dorsoventrally flattened (Fig. 1C–E). The cell length was 16.8–33.9 (22.8 ± 3.57, n = 40) μm, and the width was 9.4–18.2 (13.5 ± 2.12, n = 40) μm. A large nucleus contained a conspicuous nucleolus and located at the anterior region of the cell (Fig. 1C–E), and cells contained numerous refractile granules scattered throughout the cell (Fig. 1C–G). Brown food vacuoles containing diatoms were occasionally observed. Two unequal flagella subapically emerged from the ventral side of the cell (Fig. 1F), of which the shorter flagellum was approximately 0.5–1 times the cell length while the longer flagellum was approximately 1.2–1.5 times the cell length. Cells possessed a deep ventral groove that runs from close to the flagellar insertion point to the posterior end (Fig. 1E, G). Most cells in the culture glided on the substrate, and the shorter flagellum of gliding cells was directed anteriorly (i.e. the anterior flagellum) and beats rapidly, whereas the longer flagellum (the posterior flagellum) trailed on the substrate. Gliding cells vibrated according to the beating of the anterior flagellum. Filopodia occasionally emerged from the posterior region of the

ventral groove (Fig. 1H, I). The filopodia lacking granules, were well branched, and did not anastomose (Fig. 1H, I). When filopodia emerged from the ventral groove, both flagella were immotile and cells did not glide, and instead moved slowly along the substrate using filopodia. Cells occasionally discharged filamentous extrusomes when pressed with a cover slip, and discharged extrusomes were approximately 20–35 μm in length (Fig. 1J). Large cell clumps that reach 50 μm in diameter were occasionally observed in older cultures (Fig. 1K, L). Cells consisted of cell clumps directed outward and connected with each other by posterior end of cells (Fig. 1K). In some clumps, cells connected with a large spherical core by their posterior end (Fig. 1L).

Cells of *V. velata* were rigid, broadly ovoid, and dorsoventrally flattened, with a length of 17.5–29.7 (24.04 ± 2.69, n = 38) μm and a width of 13.1–28.1 (19.75 ± 3.32, n = 38) μm (Fig. 2A–C). Many small warts were distributed over the entire surface of the cell (Fig. 2A–C). A large nucleus with one to several nucleoli was located at the anterior region of the cell (Fig. 2A, B). Many refractile granules and non-refractile globules that appear to be oil drops were scattered throughout the cell (Fig. 2A–C), and brown food vacuoles containing diatoms were occasionally observed. One short flagellum and one long flagellum emerge subapically from the ventral side of the cell (Fig. 2B, D). The shorter flagellum was approximately 0.5–1 times the cell length, and the longer flagellum was approximately 1.2–1.5 times the cell length. Cells possessed a deep ventral groove that runs from close to the flagellar insertion point to the posterior end of the cell (Fig. 2C). Most cells in the culture glided on the substrate, and the shorter flagellum was directed anteriorly (i.e. the anterior flagellum) and beat rapidly, whereas the longer flagellum (the posterior flagellum) trailed on the substrate. Gliding cells vibrated according to the beating of the anterior flagellum. A large lamellipodium emerged from the entire region of the ventral groove that lacks granules, but filopodia occasionally emerged from the rim of the lamellipodium (Fig. 2D, E). When the

lamellipodium emerged from the ventral groove, both flagella were immotile and cells did not glide, but instead moved across the substrate using the lamellipodium. Cells occasionally discharged filamentous extrusomes when pressed with a cover slip (Fig. 2F). Discharged extrusomes were approximately 20–35 μm in length, and large cell clumps were occasionally observed in older cultures (Fig. 2G).

Electron microscopy of *V. oblonga* and *V. velata*

Scanning electron microscopy (SEM) observation showed that *V. oblonga* had two longitudinally aligned flagellar pockets (Fig. 3A), and naked anterior and posterior flagella emerge from each flagellar pocket (Fig. 3A). The cell surface was coated with granular material, and small rounded bumps were scattered on the surface (Fig. 3A, B). By contrast, the cell surface of *V. velata* was covered by fine creases and a small rounded bump was positioned at the tip of each wart (Fig. 3C, D).

Transmission electron microscopy (TEM) observations revealed that cells of *V. oblonga* were covered by a single layered theca of 30–60 nm thickness (Fig. 4A), the surface of which is covered with ambiguous material that resembles thin filaments, while the inner side of the theca is composed of electron-dense particles (Fig. 4A, B). An extrusome was located just beneath the rounded bump (Fig. 4C, 6A). Cells of *V. velata* were covered by a single layered theca of 30–60 nm thickness (Fig. 4D), the surface of which was adorned with thin ribbon-like filaments that form a pleated structure (Fig. 4D, E). The inner side of the theca was coated with electron-dense particles (Fig. 4D, E), and an extrusome was located just beneath the rounded bump (Fig. 4F, G).

The cytoplasm of *V. oblonga* was highly vacuolated, and a large nucleus with a conspicuous nucleolus was located at the anterior region of the cell (Fig. 5A). Condensed chromosomes were distributed permanently throughout the entire region of the nucleus and

surround the nucleolus (Fig. 5A). Two Golgi apparatus were located at the anterior region of the cell (Fig. 5B), and several rounded mitochondrial profiles containing tubular cristae were scattered throughout the cytoplasm (Fig. 5B, C). One or two microbodies occasionally including tubular invaginations of the cytoplasm were observed around the nucleus (Fig. 5A, B, D). Cylindrical vesicles containing dense material were observed around the basal bodies (Fig 5B, E), and one or two lattice-like structures were located near basal bodies (Fig. 5F). The extrusome, 110–150 nm in diameter and surrounded by a single membrane (Fig. 6A, B), consisted of two parts: a distal region approximately 1.2 μm in length containing an electron-dense cylindrical core, and a proximal region containing granular or lenticulate material (Fig. 6A–D). The cylindrical core appeared to be released when the extrusome is discharged (Fig. 6C). The proximal part of the extrusome was aligned in the same direction and forms clusters (Fig. 6D). The two basal bodies of *V. oblonga* were arranged approximately at a right angle (Fig. 6E), not in the same plane, while the anterior basal body was positioned at the left side of the posterior basal body. The flagellar transitional region contained four or five dense transitional plates at its distal region (Fig. 6F). A constriction of the flagellar membrane was observed at the proximal side of the transitional plates (Fig. 6F). At the distal side of the constriction, an electron-dense disk that was sandwiched by less dense transitional plates was observed (Fig. 6F). Two large and small ring structures were observed at the proximal side of the disk/plate structure (Fig. 6F).

We observed at least two striated fibers around the basal bodies of *V. oblonga*. One striated fiber (sf1) emerged from the posterior side of the posterior basal body, at the level of the cartwheel structure (Fig. 7A–C, 8D). The sf1 was broader at its origin and reached the nucleus (Fig, 7A–C, 8D). Another striated fiber (sf2) was located between the anterior and posterior basal bodies (Fig. 7E, F, 8F). A fibrillar bridge (fb) connected the proximal parts of the basal bodies (Fig. 9E). Fibrous structures other than sf1, sf2, and fb were also observed

around basal bodies. However, we could not identify all fibrous structures since they were intricately associated with each other, and their shapes and positions appeared not to be structurally conserved among cells.

Since the microtubular roots of *V. oblonga* shared clear homology with other cercozoan flagellates, we applied the same terminology used in previous studies on the cercozoan flagellar apparatus to describe them (Cavalier-Smith and Karpov 2012; Karpov 2010). The posterior basal body had a ventral posterior root that originates from the posterior flagellum (vp1), and vp1 consisted of 10 microtubules emerging from the right side of the posterior basal body that runs along the posterior flagellar pocket (Fig. 7A–D, 8A–F, 9A–F). The anterior basal body had two microtubular roots: a left root (lr) and an anterior root (ar). The lr consisted of two microtubules emerging from the left side of the anterior basal body, near the proximal end of the posterior basal body (Fig. 7B, 8G, H, 9C, D). The ar consisted of two microtubules emerging from the right side of the anterior basal body. Together, the ar and the lr lined the dorsal side of the anterior flagellar pocket (Fig. 7B, F). Several singlet microtubules indirectly associated with basal bodies were occasionally observed (Fig. 8B, C, 9A, D). Fibrous structures and microtubular roots of *V. oblonga* are illustrated in Figure 10.

Molecular phylogenetic analysis

Molecular phylogenetic analysis using SSU rRNA genes showed that *V. oblonga* and *V. velata* formed a clade with two *Ventrifissura* species and several environmental sequences with high statistical support; the bootstrap probability (BP) was 98%, and the Bayesian posterior probability (BPP) was 1. The *Ventrifissura* clade separated into two subclades: a moderately supported (BP = 54%, BPP = 1) subclade comprising *V. oblonga*, *V. velata*, and an environmental sequence derived from seawater, and a robust clade (BP = 93%, BPP = 1) including *V. artocarpoidea*, *V. foliiformis*, and three marine environmental sequences. The *Ventrifissura* clade branched as a sister to an environmental clade named “eVentri” in Scoble

and Cavalier-Smith (2014). Monophyly of eVentri and *Ventrifissura* was strongly supported (BP = 93%, BPP = 1), and these were placed as the most basal lineage of Imbricatea, but this position was not well supported (BP = 6% and no BPP due to differences in topology).

To elucidate the possible position of *Ventrifissura*, approximately unbiased (AU) tests were performed against six different tree topologies (Table 1). Monophyly of *Ventrifissura* and Imbricatea (tree 1) and monophyly of *Ventrifissura* and Thecofilosea (tree 2) were not rejected by the AU tests, whereas monophyly of *Ventrifissura* and *Metromonas simplex* (tree 4), monophyly of *Ventrifissura* and *Micrometopion nutans* (tree 5), and *Ventrifissura* branching outside of Ventrifilosa (tree 3) were rejected at the 5% significance level.

Discussion

Justification of new species

In our molecular phylogenetic analysis, *V. oblonga* and *V. velata* were included in the *Ventrifissura* clade with robust support. *Ventrifissura oblonga*, *V. velata*, and another two *Ventrifissura* spp. were placed in distinct phylogenetic positions in the *Ventrifissura* clade. The morphological characteristics of *Ventrifissura* spp. are summarized in Table 2. They share common morphological and behavioral characteristics such as gliding locomotion, a dorsoventrally flattened cell shape, and the presence of a ventral groove. Additionally, both *V. oblonga* and *V. velata* can be distinguished from other species by morphological characteristics. The cell of *V. oblonga* is more slender than that of other *Ventrifissura* spp., and unlike other species *V. velata* has lamellipodia. *Ventrifissura oblonga* and *V. velata* are similar in terms of cell size, but they are twice as small as *V. artocarpoidea* and *V. foliiformis*. *Ventrifissura* possess two types of surface structures, smooth and warty surfaces. *Ventrifissura oblonga* has a smooth surface like *V. foliiformis*, while *V. velata* has a warty

surface similar to *V. artocarpoidea*. Our molecular phylogenetic analysis revealed a close relationship between *V. oblonga* and *V. velata*, indicating that the surface structure could be changed easily along with diversification, providing a useful characteristic for distinguishing each species. Based on molecular phylogenetic analysis and morphological comparison, we conclude that the two strains should be treated as new species of *Ventrifissura*, named *V. oblonga* and *V. velata*.

Ventrifissura is a basal member of Thecofilosea

Ventrifissura is one of poorly studied cercozoan flagellates lacking ultrastructural information. In Cercozoa, there is a large variety of structures including cell and flagellar surface appendages, extrusomes, mitochondria, and other organelle structures, and the number and arrangement of microtubular and non-microtubular roots in the flagellar apparatus. Several ultrastructural characteristics are shared among specific lineages of Cercozoa, and are important traits for elucidating phylogenetic relationships. Herein, we compare ultrastructure elements of *Ventrifissura* with those of other cercozoans and discuss the placement of *Ventrifissura* within Cercozoa.

Ventrifissura possess a smooth monolayered theca with an inner surface coated with amorphous material and an outer surface lined with dense particles. In Cercozoa, Thecofilosea and Metromonadea are known as thecate groups. The theca of Metromonadea is a delicate monolayer or bilayer covered with fibrous material (Mylnikov et al. 1999; Mylnikova and Mylnikov 2011), whereas thecae of Thecofilosea are typically rigid and vary in terms of thickness and the number of layers present (Hargraves 2002; Hoppenrath and Leander 2006a; Swanberg et al. 1986; Tomsen et al. 1991; Yabuki and Ishida 2011). The theca of *Ventrifissura* is similar to that of Metromonadea in terms of possessing fibrous material on both sides, although the theca of Metromonadea are thinner and less electron-dense. Since phylogenetic analyses revealed no close relationship between *Ventrifissura* and

249 Metromonadea, their similar thecate structures probably do not share the same origin. Indeed,
250 other thecofilosean flagellates such as *Ebria tripartita* and *Hermesinum adriaticum* have a
251 relatively thin monolayer theca with fibrous material on the outer surface (Hargraves 2002).
252 Therefore, the thinner thecae of *Ventrifissura* and ebriids are more similar to those of
253 thecofiloseans, and this may reflect the ancestral state of Thecofilosea, and 'higher evolved'
254 Thecofilosea have smooth thecae, some of which include extrusomes in their theca, such as
255 *Protaspa* and *Cryothecomonas*. A condensed chromosome is another characteristic shared
256 with most thecofilosean organisms (Drebes et al. 1996; Hargraves 2002; Hoppenrath and
257 Leander 2006a; Shiratori and Ishida 2016; Swanberg et al. 1986; Yabuki and Ishida 2011)
258 and probably one of the ancestral thecofilosean characteristics. In addition, flagella that are
259 inserted from different flagellar pockets are also shared exclusively among *Ventrifissura* and
260 Thecofilosea in Cercozoa (Hoppenrath and Leander 2006a; Schnepf and Kühn 2000).
261 Extrusomes are widely reported in various cercozoans and display broad diversity in terms
262 of size and structure. Most thecofilosean flagellates such as *Cryothecomonas*, *Mataza*, and
263 *Protaspa* have very slender cylindrical extrusomes similar to those in *Ventrifissura*
264 (Hoppenrath and Leander 2006a; Schnepf and Kühn 2000; Tomsen et al. 1991; Yabuki and
265 Ishida 2011). Slender extrusomes are also observed in non-thecofilosean cercozoans such as
266 Thaumatomonadida and Metromonadea. In Thaumatomonadida, slender extrusomes are
267 reported in *Ovaloplaca* and *Esquamula* but they are dissimilar to that of thecofiloseans since
268 they have a striped pattern and a non-cylindrical structure (Ota et al. 2012; Shiratori et al.
269 2012). Extrusomes of Metromonadea are similar to those of thecofiloseans in their cylindrical
270 structure, but they exhibit a wheel-shaped pattern in cross-sections and are shorter than
271 thecofilosean extrusomes (Mylnikov et al. 1999; Mylnikova and Mylnikov 2011).
272 Although our SSU rRNA gene tree could not resolve the phylogenetic position of
273 *Ventrifissura*, similar to previous studies, our AU tests rejected the monophyly of

Ventrifissura and Metromonadea (i.e., *Metromonas simplex* and *Micrometopion nutans*, respectively). AU tests also rejected a hypothesis that *Ventrifissura* branches outside of Ventrifilosa. In Ventrifilosa, there are no amoeba or flagellate with a rigid theca, or slender extrusomes of cylindrical structure, other than Thecofilosea. Therefore, it seems most parsimonious that Thecofilosea and *Ventrifissura* are monophyletic. Based on the results of molecular phylogenetic analyses and ultrastructural observations, we conclude that *Ventrifissura* is a basal lineage of Thecofilosea, as classified by Howe et al. (2011).

Our ultrastructural observation of *Ventrifissura* also revealed several other characteristics that can help us understand the ultrastructural diversity and evolution of Thecofilosea. A narrow thecal funnel in the flagellar pit is a specific characteristic of cryomonad flagellates (Drebes et al. 1996; Hoppenrath and Leander 2006a; Schnepf and Kühn 2000; Tomsen et al. 1991). The Ebriid flagellate *Hermesinum adriaticum* also has a funnel-like thickened portion of the theca around the flagellar insertion point (Hargraves 2002), whereas *Mataza* and *Ventrifissura* lack this funnel or a similar structure (Yabuki and Ishida 2011; this study). This suggests that the funnel is a derived characteristic of Thecofilosea and was probably acquired at the common ancestor of cryomonads and ebriids. The cylindrical vesicles containing dense material is unique structure found in *V. oblonga*. Although we could not observe discharged vesicles, as in spherical vesicles in chlorarachniophytes, it may contain theca materials and involve with theca formation (Ishida and Hara 1994). The lattice structure is also not observed in Cercozoa. It looks like euglenozoan paraxonemal rod that associated with flagella but is located anterior region of the cell. Further studies on these structures are needed to determine their biological function.

The flagellar apparatus of Thecofilosea is only reconstructed in *Cryothecomonas aestivalis* and *Protaspa longipes*. Both have a simple flagellar apparatus that consists of a single microtubular band corresponding to vp1, and a fibrillar bridge that connects basal

bodies (Drebes et al. 1996; Schnepf and Kühn 2000). Many singlet microtubules indirectly associated with basal bodies are also present in both species. Other flagellates in Ventrifilosa have more complex microtubular root systems that typically consist of four microtubular roots: ar, lr, vp1, and a ventral posterior root that originates from the anterior basal body (vp2) (Cavalier-Smith and Karpov 2012; Cavalier-Smith and Oates 2012; Karpov 2010). Our ultrastructural observation showed that the flagellar apparatus of *Ventrifissura* shares similar characteristics with those of cryomonads, such as singlet microtubules that are situated around right-angled basal bodies, and a connecting fiber that connects the proximal ends of basal bodies (Drebes et al. 1996; Schnepf and Kühn 2000). *Ventrifissura* lacks vp2 as in cryomonad flagellates, but it retains other three microtubular roots. Microtubular root plays various function such as for feeding, locomotion, and supporting the cell body as cytoskeleton (Moestrup 1982). The vp2 is also believed to support the ventral portion of the cell, together with vp1 (Cavalier-Smith and Karpov 2012). Ancestral thecofilosean flagellates possibly lost vp2 by acquiring a rigid extracellular theca that supports the cell body. In contrast to cryomonads, *V. oblonga* possesses the da and the lr. Therefore, the less reduced microtubular roots of *Ventrifissura* may represent the ancestral state of Thecofilosea.

Taxonomic Treatment

Phylum Cercozoa Cavalier-Smith, 2003

Class Thecofilosea Cavalier-Smith, 2003

Order Ventricleftida Howe et al., 2011

Family Ventrifissuridae Cavalier-Smith et al., 2018

Genus *Ventrifissura* Chantangsi and Leander, 2010

Revised diagnosis: Uninucleate marine gliding biflagellate with a rigid extracellular theca. Cells ovoid or obovoid and dorsoventrally flattened. Cells either with smooth surfaces or with numerous pointed warts. Circular to oblong-shaped nucleus located at the anterior end

of the cell. Ventral groove present. Filopodia or lamellipodia present. Theca a monolayer structure covered with filamentous material. Flagella inserted subapically. Some species with an anterior protrusion. Highly slender extrusomes present. Lacking a funnel in the flagellar pit.

***Ventrifissura oblonga* Shiratori, Yabuki, Ishida sp. nov. (ICZN)**

Diagnosis: Cells ovoid, 16.8–33.9 μm in length and 9.4–18.2 μm in width. Cells slightly dorsoventrally flattened with a smooth surface. Filopodia emerging from a ventral groove. Outer surface of theca covered with thin filaments.

Hapantotype: One microscope slide (TNS-AL-58968s), deposited in the herbarium of the National Museum of Nature and Science (TNS), Tokyo, Japan.

Paratype: One EM block (TNS-AL-58968tb) deposited in the TNS. These cells are derived from the same sample as the holotype.

DNA sequence: Small subunit ribosomal RNA gene, LC375249.

Type locality: Seawater from a wharf in Tokyo Bay, Japan (latitude = 35.6281°N, longitude = 139.7713°E).

Collection date: July 6, 2012.

Authentic culture: The strain SRT122 used for describing this species is deposited and is maintained at the National Institute for the Environmental Sciences, Tokyo, Japan, under accession NIES-4233.

Etymology: *oblong* (oval) refers to the cell shape of this organism.

ZooBank LSID: urn:lsid:zoobank.org:act:20647F45-38E9-4B89-A99A-38C421645D10

***Ventrifissura velata* sp. nov. Shiratori, Yabuki, Ishida sp. nov. (ICZN)**

Diagnosis: Cells broadly ovoid, 17.5–29.7 μm in length and 13.1–28.1 μm in width. Cells dorsoventrally flattened and with numerous pointed warts on the surface. Lamellipodia

emerging from a ventral groove. Outer surface of the theca covered with aligned thin ribbon-like filaments that form a pleated structure.

Hapantotype: One microscope slide (TNS-AL-58968s), deposited in the herbarium of the National Museum of Nature and Science (TNS), Tokyo, Japan.

Paratype: One EM block (TNS-AL-58968tb) deposited in the TNS. These cells are derived from the same sample as the holotype.

DNA sequence: Small subunit ribosomal RNA gene, LC375250.

Type locality: Sand sample from Oarai Sun Beach, Ibaraki, Japan (latitude = 36.3013°N, longitude = 140.5700°E).

Collection date: July 10, 2011.

Etymology: *velum* (veil) refers to the morphology of the pseudopodia.

ZooBank LSID: urn:lsid:zoobank.org:act:530EC8C5-8E4D-4F71-B6B8-FEE0833647A1

Materials and Methods

Culture establishment

Cells of *Ventrifissura oblonga* n. sp. were isolated from a seawater sample from Tokyo Bay, Tokyo, Japan (35.6281°N, 139.7713°E) on July 30, 2011. Cells of *Ventrifissura velata* n. sp. were isolated from a sand sample from Oarai Sun Beach, Ibaraki, Japan (36.3013°N, 140.5700°E) on July 6, 2012. Clonal cultures of *V. oblonga* (strain SRT122) and *V. velata* (strain SRT224) were established by the single-cell isolation technique using micropipettes. Each culture was maintained in ESM medium (Kasai et al. 2009) with pennate diatoms as food at 18°C under a 14 h light/10 h dark cycle. Strain SRT224 was extinct in July 2016. *Ventrifissura oblonga* (strain SRT122) was deposited at the National Institute for the Environmental Sciences (NIES), Tsukuba, Japan, under accession NIES-xxxx.

Light microscopy observation

374 Cells of *V. oblonga* and *V. velata* were observed in glass bottom dishes or on glass slides
375 covered with a cover slip using an Olympus IX71 inverted microscope (Olympus, Tokyo,
376 Japan) equipped with an Olympus DP73 CCD camera (Olympus).

377 **Scanning electron microscopy**

378 Cell suspensions of strains SRT122 and SRT224 were mounted on 8.5 mm diameter glass
379 SEM plates (Okenshoji Co., Tokyo, Japan) coated with 0.1% (w/v) poly-L-lysine and
380 subsequently fixed using 4% (w/v) osmium tetroxide (OsO_4) vapor for 30 min at room
381 temperature. Cells on glass SEM plates were post-fixed with 1% (w/v) osmium tetroxide in
382 0.2 M cacodylate buffer (pH 7.2) for 2 h at room temperature. Fixed cells were gradually
383 dehydrated using a graded ethanol series of 15−100% ethanol. After dehydration, specimens
384 were placed in a 1:1 mixture of 100% ethanol and t-butyl alcohol followed by pure t-butyl
385 alcohol twice and chilled in a freezer. Specimens were freeze-dried using a VFD-21S freeze
386 drier (SHINKU-DEVICE, Ibaraki, Japan) and mounted on aluminum stubs using carbon
387 paste. Specimens were sputter-coated with platinum-palladium using a Hitachi E-102 sputter-
388 coating unit (Hitachi High-Technologies Corp., Tokyo, Japan) and observed using a JSM-
389 6360F field emission SEM instrument (JEOL, Tokyo, Japan).

390 **Transmission electron microscopy**

391 Specimens for TEM observation were prepared by fixing cells of strains SRT122 and SRT224
392 using an equal amount of 2% (v/v) glutaraldehyde in filtered and sterilized natural seawater
393 for 1 h at room temperature for pre-fixation. Cells were collected by centrifugation, and cell
394 pellets were washed with seawater three times. Cells were then post-fixed with 1% (v/v)
395 OsO_4 in seawater, and dehydration was performed using a graded series of 30−100% ethanol
396 (v/v). After dehydration, cells were placed in a 1:1 mixture of 100% ethanol and acetone
397 followed by pure acetone twice. Resin replacement was performed using a 1:1 mixture of
398 acetone and Agar Low Viscosity Resin R1078 (Agar Scientific Ltd, Stansted, UK), followed

by pure resin. Resin was polymerized by heating at 60°C for 12 h. Ultrathin sections were prepared on a Reichert Ultracut S ultramicrotome (Leica, Vienna, Austria), double-stained with 2% (w/v) uranyl acetate and lead citrate (Hanaichi et al. 1986; Sato 1968), and observed using a Hitachi H-7650 electron microscope (Hitachi High-Technologies Corp) equipped with a Veleta TEM CCD camera (Olympus).

DNA extraction and PCR amplification

Total DNA from strains SRT122 and SRT224 was extracted from cell pellets collected by centrifugation using a DNeasy Plant mini kit (Qiagen Science, Valencia, CA) according to the manufacturer's instructions. SSU rRNA from each strain was amplified by PCR with primers 18F and 18R (Yabuki et al. 2010). Amplification involved 30 cycles of denaturation at 94°C for 30 s, annealing at 55°C for 30 s, and extension at 72°C for 2 min, followed by an additional extension for 2 min at 72°C at the end of the reaction. Amplified DNA fragments were purified after gel electrophoreses with a QIAquick Gel Extraction Kit (Qiagen Science), then cloned into the pGEM T-easy vector (Promega, Tokyo, Japan). Inserted DNA fragments were sequenced in full using a 3130 Genetic Analyzer (Applied Biosystems, Monza, Italy) with a BigDye Terminator v3.1 cycle sequencing kit (Applied Biosystems). SSU rRNA gene sequences of strains SRT122 and SRT224 have been deposited in GenBank under accession codes xxxx and yyyy, respectively.

Sequence alignment and molecular phylogenetic analysis

For phylogenetic analysis, we obtained cercozoan SSU rRNA gene sequences from the NCBI database and created a dataset. SSU rRNA gene sequences of strains SRT122 and SRT224 were then added to the dataset, and automatic alignment was performed using MAFFT v7.394 (Katoh and Standley 2013), followed by manual alignment with SeaView v4.6 (Gouy et al. 2010). Ambiguously aligned regions were manually deleted to get a final alignment containing 1,661 sites of 91 OTUs. A maximum-likelihood (ML) tree was constructed using

RAxML v.8.2.4 (Stamatakis 2014) based on the GTR+Γ model. Tree searches began with 20 randomized maximum-parsimony trees, and the highest log-likelihood (lnL) was selected as the ML tree. A non-parametric bootstrap analysis (1,000 replicates) was conducted using the GTR+Γ model, and a Bayesian analysis was carried out using MrBayes v.3.2.6 (Ronquist et al. 2012), also with the GTR+Γ model. One cold and three heated Markov chain Monte Carlo simulations with default chain temperatures were run for 1.5×10^6 generations, sampling lnL values and trees at 100-generation intervals. Convergence was assessed by the average standard deviation of split frequencies, and the first 25% of the total generations of each analysis were discarded as 'burn-in'. BPP and branch lengths were calculated from the remaining trees.

For AU tests, five alternative trees were constructed using RAxML with the same parameters as above. Per site log-likelihood scores were calculated using RAxML with the GTR+Γ model, and the site-wise log-likelihood of each tree was analyzed using CONSELv0.20 (Shimodaira and Hasegawa 2001).

Acknowledgments

This work was supported by JSPS KAKENHI Grant Number 13J00587 and 18J02091.

References

Cavalier-Smith T, Chao EE (2003) Phylogeny and classification of phylum Cercozoa (Protozoa). Protist **154**:341–358

Cavalier-Smith T, Chao EE, Lewis R (2018) Multigene phylogeny and cell evolution of chromist infrakingdom Rhizaria: contrasting cell organisation of sister phyla Cercozoa and Retaria. Protoplasma https://doi.org/10.1007/s00709-018-1241-1

448 **Cavalier-Smith T, Karpov SA** (2012) *Paracercomonas* kinetid ultrastructure, origins of the
449 body plan of Cercomonadida, and cytoskeleton evolution in Cercozoa. Protist **163**:47–75

450 **Cavalier-Smith T, Oates B** (2012) Ultrastructure of *Allapsa vibrans* and the body plan of
451 Glissomonadida (Cercozoa). Protist **163**:165–187

452 **Chantangsi C, Leander BS** (2010a) An SSU rDNA barcoding approach to the diversity of
453 marine interstitial cercozoans, including descriptions of four novel genera and nine novel
454 species. Int J Syst Evol Microbiol **60**:1962–1977

455 **Chantangsi C, Leander BS** (2010b) Ultrastructure, life cycle and molecular phylogenetic
456 position of a novel marine sand-dwelling cercozoan: *Clautriavia biflagellata* sp. nov. Protist
457 161:133–147

458 **Drebes G, Kühn SF, Gmelch A, Schnepf E** (1996) *Cryothecomonas aestivalis* sp. nov., a
459 colourless nanoflagellate feeding on the marine centric diatom Guinardia delicatula (Cleve)
460 Hasle. Helgoländer Meeresunters **50**:497—515

461 **Dumack K, Bonkowski M, Clauß S, Völcker E** (2018) Phylogeny and Redescription of the
462 Testate Amoeba *Diaphoropodon archeri* (Chlamydophryidae, Thecofilosea, Cercozoa), De
463 Saedeleer 1934, and Annotations on the Polyphyly of Testate Amoebae with Agglutinated
464 Tests in the Cercozoa. J Eukaryot Microbiol **65**:308–314

465 **Dumack K, Öztoprak H, Rüger L, Bonkowski M** (2017) Shedding light on the
466 polyphyletic thecate amoeba genus *Plagiophrys*: Transition of some of its species to
467 Rhizaspis (Tectofilosida, Thecofilosea, Cercozoa) and the establishment of *Sacciforma* gen.
468 nov. and Rhogostomidae fam. nov. (Cryomonadida, Thecofilosea, Cercozoa). Protist **168**:92–
469 108

Gouy M, Guindon S, Gascuel O (2010) SeaView version 4: a multiplatform graphical user interface for sequence alignment and phylogenetic tree building. Mol Biol Evol **27:**221–224

Hanaichi T, Sato T, Hoshino M, Mizuno N (1986) A stable lead stain by modification of Sato's method. Proceedings of the XIth International Congress on Electron Microscopy, Japanese Society for Electron Microscopy, Kyoto, Japan, pp. 2181–2182

Hargraves PE (2002) The ebridian flagellates *Ebria* and *Hermesium*. Plankton Biol Ecol **49**: 9–16

Hoppenrath M, Leander BS (2006a) Dinoflagellate, euglenid, or cercomonad? The ultrastructure and molecular phylogenetic position of *Protaspis grandis* n. sp. J Eukaryot Microbiol **53**:327–342

Hoppenrath M, Leander BS (2006b) Ebriid phylogeny and the expansion of the Cercozoa. Protist **157**: 279–290

Howe A, Bass D, Scoble J, Lewis R, Vickerman K, Arndt H, Cavalier-Smith T (2011) Novel cultured protists identify deep-branching environmental DNA clades of Cercozoa: new genera *Tremula*, *Micrometopion*, *Minimassisteria*, *Nudifila*, *Peregrinia*. Protist **162**:332–372

Karpov SA (2010) Flagellar apparatus structure of *Thaumatomonas* (Thaumatomonadida) and thaumatomonad relationships. Protistology **6**:326–344

Kasai F, Kawachi M, Erata M, Mori F, Yumoto K, Sato M, Ishimoto M (2009) NIES-Collection. List of strains. (8th ed.). Jpn J Phycol (Sôrui) **57**:1–350

Katoh K, Standley DM (2013) MAFFT multiple sequence alignment software version 7: improvements in performance and usability. Mol Biol Evol 30:772–780

Moestrup Ø (1982) Flagellar structure in algae: a review, with new observations particularly on the Chrysophyceae, Phaeophyceae (Fucophyceae), Euglenophyceae and Reckertia. Phycologia **21**:427–528

Mylnikova AP, Mylnikov ZM (2011) Ultrastructure of the Marine Predatory Flagellate *Metromonas simplex* Larsen et Patterson, 1990 (Cercozoa). Inland Water Biol **4**:5–10

Mylnikov AP, Mylnikova ZM, Tsvetkov AI (1999) Ultrastructure of the predatory marine flagellate *Metopion fluens*. Tsitologiia **41**:581–585

Ota S, Eikrem W, Edvardsen B (2012) Ultrastructure and molecular phylogeny of thaumatomonads (Cercozoa) with emphasis on *Thaumatomastix salina* from Oslofjorden, Norway. Protist **163**:560–573

Ronquist F, Teslenko M, von der Mark P, Ayres DL, Darlig A, Höhna S, Larget B, Liu L, Suchard MA, Huelsenbeck JP (2012) MrBayes 3.2: efficient Bayesian phylogenetic inference and model choice across a large model space. Syst Biol 61:539–542

Sato T (1968) A modified method for lead staining of thin sections. J Electron Microsc **17**:158–159

Schnepf E, Kühn SF (2000) Food uptake and fine structure of *Cryothecomonas longipes* sp. nov., a marine nanoflagellate incertae sedis feeding phagotrophically on large diatoms. Helgol Mar Res **54**:18–32

Scoble J. M, Cavalier-Smith T (2014). Scale evolution, sequence phylogeny, and taxonomy of thaumatomonad Cercozoa: 11 new species and new genera *Scutellomonas*, *Cowlomonas*, *Thaumatospina* and *Ovaloplaca*. European Journal of Protistology **50**:270–313

Shimodaira H, Hasegawa M (2001) CONSEL: for assessing the confidence of phylogenetic tree selection. Bioinformatics 17:1246–1247

Shiratori, T, Ishida K (2016). *Trachyrhizium urniformis* n. g., n. sp., a Novel Marine Filose Thecate Amoeba Related to a Cercozoan Environmental Clade (Novel Clade 4). Journal of Eukaryotic Microbiology **63**:722–731

Shiratori T, Yabuki A, Ishida K (2012) *Esquamula lacrimiformis* n. g., n. sp., a new member of thaumatomonads that lacks siliceous scales. J Eukaryot Microbiol **59**: 527–536

Stamatakis A (2014) RAxML Version 8: A tool for Phylogenetic Analysis and Post-Analysis of Large Phylogenies. Bioinformatics **30**:1312–1313

Swanberg N, Bennett P, Lindsey JL, Anderson OR (1986) The biology of a coelodendrid: amesopelagic phaeodarian radiolarian. Deep-Sea Res **33**:15–25

Thomsen HA, Buck KR, Bolt PA, Garrison DA (1991) Fine structure and biology of *Cryothecomonas* gen. nov. (Protista incertae sedis) from the ice biota. Can J Zool **69**:1048–1070

Yabuki A, Inagaki Y, Ishida K (2010) *Palpitomonas bilix* gen. et sp. nov.: a novel deep-branching heterotroph possibly related to Archaeplastida or Hacrobia. Protist **161**:523–538

Yabuki A, Ishida K (2011) *Mataza hastifera* n. g., n. sp.: a possible new lineage in the Thecofilosea (Cercozoa). J Eukaryot Microbiol **58**:94–102

Yuasa T, Takahashi O, Dolven JK, Mayama S, Matsuoka A, Honda D, Bjørklund KR (2006) Phylogenetic position of the small solitary phaeodarians (Radiolaria) based on 18S rDNA sequences by single cell PCR analysis. Marine Micropaleontol **59**:104–114

533

534

535 **Table 1. Approximately unbiased (AU) tests with different tree topologies**

Tree ID	Tree topology	*p*-value
1	Monophyly of *Ventrifissura*[1] and Imbricatea	0.678
2	Monophyly of *Ventrifissura* and Thecofilosea	0.595
3*	Monophyly of Ventrifilosa[2] without *Ventrifissura*	0.044
4*	Monophyly of *Ventrifissura* and *Micrometopion nutans*	0.030
5*	Monophyly of *Ventrifissura* and *Metromonas simplex*	1e-04

536 * Trees rejected at the 5% significance level.

537 [1] (four species of *Ventrifissura* and 16 related environmental sequences).

538 [2] (Imbricatea, Sarcomonadea, and Thecofilosea).

539

Table 2. Comparison of the morphological characteristics of *Ventrifissura* spp.

	V. oblonga n. sp.	*V. velata* n. sp.	*V. artocarpoidea*	*V. foliiformis*
Cell size; length (μm)	16.8–33.9	17.5–29.7	43–45	40–47
width (μm)	9.4–18.2	13.1–28.1	35–36	30–35
Cell shape	ovoid, slightly dorsoventrally flattened	broadly ovoid, dorsoventrally flattened	broadly obovoid, slightly dorsoventrally flattened	broadly obovoid, extremely dorsoventrally flattened
Cell surface	smooth	warty	warty	smooth
Flagellar insertion	subapically	subapically	subapically	subapically
Pseudopodia	filopodia	lamellipodium	not reported	filopodia
Locomotion	gliding	gliding	gliding	gliding
Position of nucleus	anterior end	anterior end	anterior end	anterior end
Ventral groove	present	present	present	present

Figure legends

Figure 1

Differential interference contrast (DIC) micrographs of *Ventrifissura oblonga* n. sp. AF, anterior flagellum; FV, food vacuole; N, nucleus; n, nucleolus; PF, posterior flagellum; VG, ventral groove. **A.** The schematic drawing viewed from ventral side of the cell. **B.** The schematic drawing viewed from left side of the cell. **C, D.** Ventral view of living cells. **E.** Lateral view of living cells. **F.** Ventral view of living cells, showing two unequal flagella. **G.** Ventral view of living cells, showing ventral groove. **H, I.** Filose pseudopodia emerging from the ventral groove. **J.** Cells with discharged extrusomes. **K, L.** Colony-like cell cluster. Scale bar: A–G = 10 μm; I and J = 50 μm.

Figure 2

Differential interference contrast (DIC) micrographs of *Ventrifissura velata* n. sp. AF, anterior flagellum; FV, food vacuole; N, nucleus; n, nucleolus; PF, posterior flagellum; VG, ventral groove. **A.** Ventral view of living cells. **B.** Lateral view of living cells. **C.** Ventral view of living cells, showing ventral groove. **D, E.** Lamellipodia emerging from the ventral groove. **F.** Cells with discharged extrusomes. **G.** Colony-like cell cluster. Scale bars: A–F = 10 μm; G = 50 μm.

Figure 3

Scanning electron micrographs of *Ventrifissura oblonga* n. sp. (A, B) and *Ventrifissura velata* n. sp. (C, D). AF, anterior flagellum; PF, posterior flagellum; VG, ventral groove. Triple arrowheads indicate rounded bumps. **A.** Whole-cell micrograph of *V. oblonga*. **B.** Cell surface of *V. oblonga*. **C.** Whole-cell micrograph of *V. velata*. **D.** Cell surface of *V. velata*. Scale bars: A and C = 5 μm; B and D = 1 μm.

Figure 4

Transmission electron micrographs of *Ventrifissura oblonga* n. sp. (A–C) and *Ventrifissura velata* n. sp. (D–G). Arrowheads indicate filamentous material on the outer surface of the theca. Double arrowheads indicate dense particles at the inner side of the theca. Triple arrowheads indicate rounded bumps. **A.** Transverse section of the extracellular theca of *V. oblonga*. **B.** Tangential section of the theca of *V. oblonga*. **C.** Extracellular theca showing a rounded bump just above an extrusome of *V. oblonga*. **D.** Transverse section of the extracellular theca of *V. velata*. **E.** Tangential section of the theca of *V. velata*. **F.** Extracellular theca showing a rounded bump just above an extrusome of *V. velata*. **G.** Discharged extrusome of *V. velata*. Scale bars: A–C and F = 500 nm; D, E, and G = 1 μm.

Figure 5

Transmission electron micrographs of *Ventrifissura oblonga* n. sp. AF, anterior flagellum; G, Golgi apparatus; M, mitochondria; MB, microbody; N, nucleus; n, nucleolus; PF, posterior flagellum. Asterisks indicate elongate vesicles containing dense material. **A.** General cell image. **B.** Anterior portion of the cell. **C.** Mitochondria with tubular cristae. **D.** Microbody with tubular invagination of cytoplasm. **E.** Anterior portion of the cell showing cylindrical vesicles. **F.** Lattice-like structures near basal bodies. Scale bars: A = 5 μm; B and D–F = 1 μm; C = 500 nm.

Figure 6

Transmission electron micrographs of *Ventrifissura oblonga* n. sp. D, disk sandwiched by two transitional plates; N, nucleus; R, transitional ring. Thin arrowheads indicate transitional plates. Triple arrowhead indicates rounded bumps. **A.** Longitudinal section of slender

extrusomes. **B.** Cross-section of slender extrusomes. **C.** Longitudinal section of discharged extrusomes. **D.** Profiles of different extrusomes in the cytoplasm. **E.** High magnification view of two basal bodies. **F.** High magnification view of the basal body and transitional region. Scale bars: A–C and F = 500 nm; D and E = 1 μm.

Figure 7

Transmission electron micrographs of *Ventrifissura oblonga* n. sp. AB, anterior basal body; ar, anterior root; fb, fibrillar bridge; lr, left root; N, nucleus; PB, posterior basal body; sf1, striated fiber 1; sf2, striated fiber 2; vp1, ventral posterior root originating from the posterior basal body. **A–F.** Selected serial section around basal bodies. Viewed from left to right. Scale bar = 1 μm.

Figure 8

Transmission electron micrographs of *Ventrifissura oblonga* n. sp. AB, anterior basal body; fb, fibrillar bridge; lr, left root; PB, posterior basal body; sf1, striated fiber 1; sf2, striated fiber 2; vp1, ventral posterior root originating from the posterior basal body. Arrows indicate singlet microtubules around basal bodies. **A–H.** Selected serial section around basal bodies. Viewed from ventral to dorsal. Scale bar = 500 nm.

Figure 9

Transmission electron micrographs of *Ventrifissura oblonga* n. sp. AB, anterior basal body; ar, anterior root; fb, fibrillar bridge; lr, left root; PB, posterior basal body; sf1, striated fiber 1; sf2, striated fiber 2; vp1, ventral posterior root originating from the posterior basal body. **A-H.** Selected serial section around basal bodies. Viewed from ventral posterior to dorsal anterior. Scale bar = 1 μm.

Figure 10

Illustration of the flagellar apparatus of *Ventrifissura oblonga* n. sp. AB, anterior basal body; ar, anterior root; fb, fibrillar bridge; lr, left root; PB, posterior basal body; sf1, striated fiber 1; sf2, striated fiber 2; vp1, ventral posterior root originating from the posterior basal body. Presumed universal terminologies of the microtubular roots are shown in brackets.

Figure 11

Maximum-likelihood tree of 85 filosans and six endomyxans using 1,661 positions of the small subunit (SSU) rRNA gene sequences. Environmental sequences are labeled only with accession numbers. Values at each branch indicate the bootstrap probability (≥50% shown). Bold branches indicate Bayesian posterior probabilities ≥0.95.

Figure 1

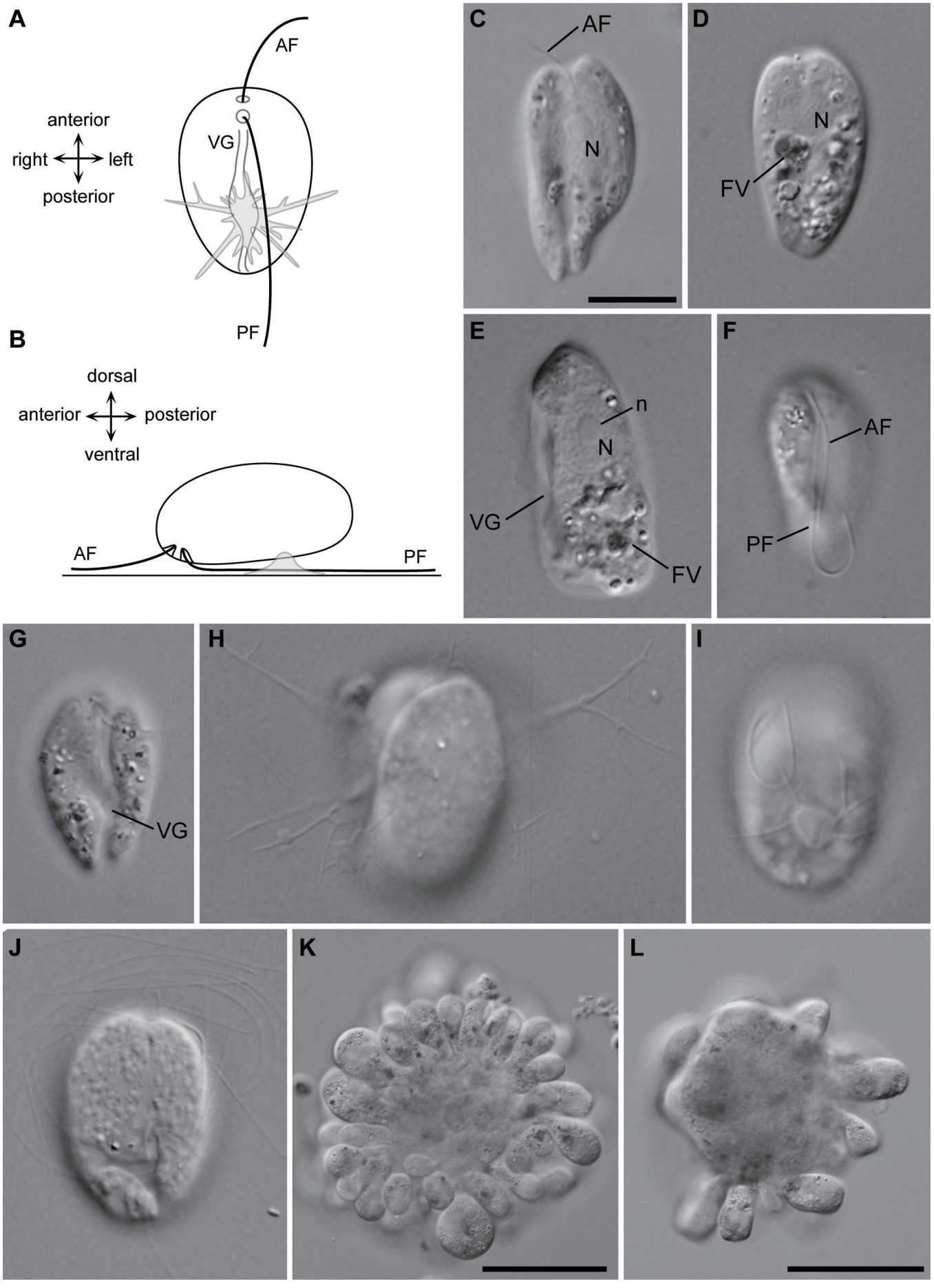
A
AF
anterior
right
left
posterior
VG
PF
B
dorsal
anterior
posterior
ventral
AF
PF
C
AF
N
D
N
FV
E
n
N
VG
FV
F
AF
PF
G
VG
H
I
J
K
L

Figure 2

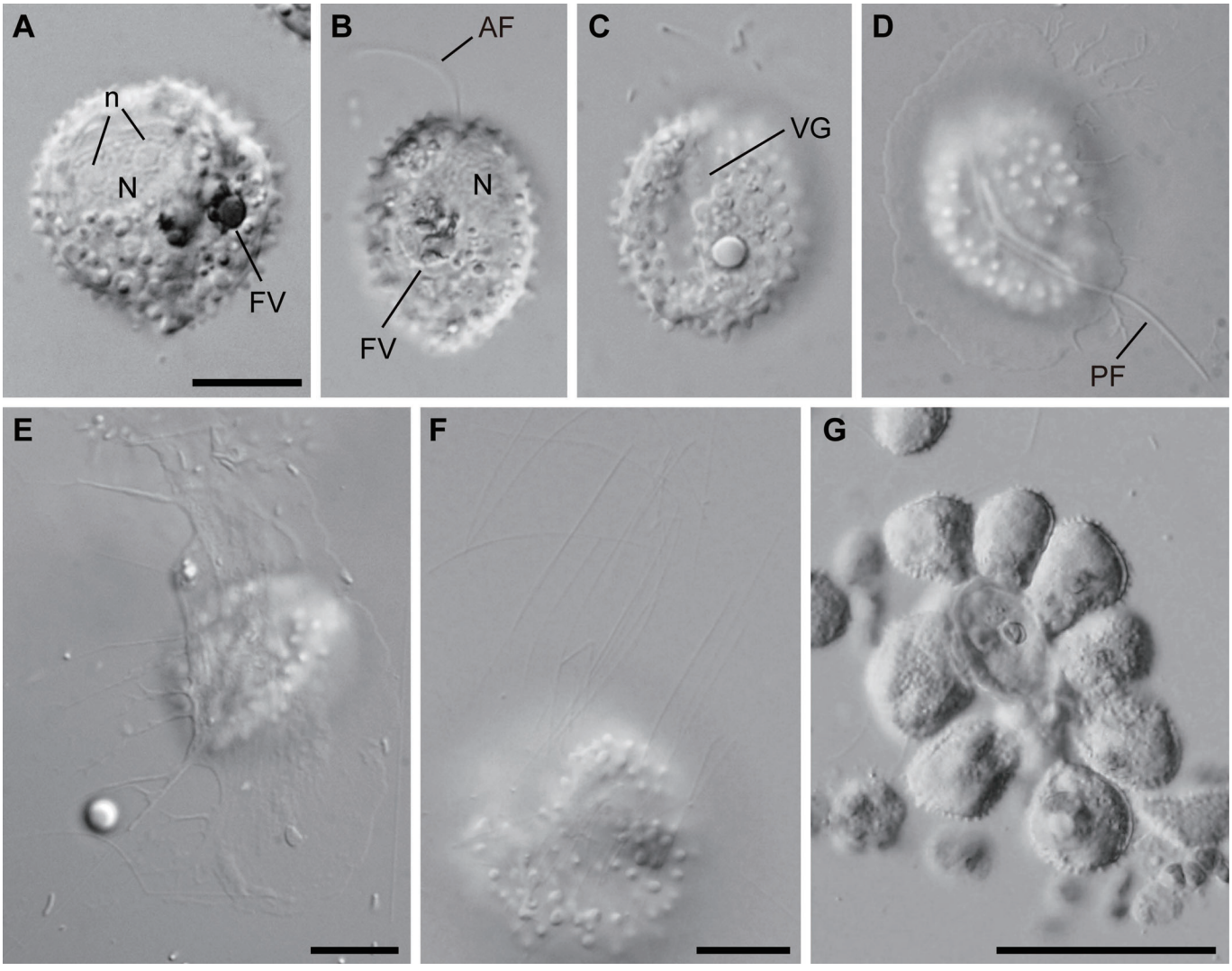

Figure 3

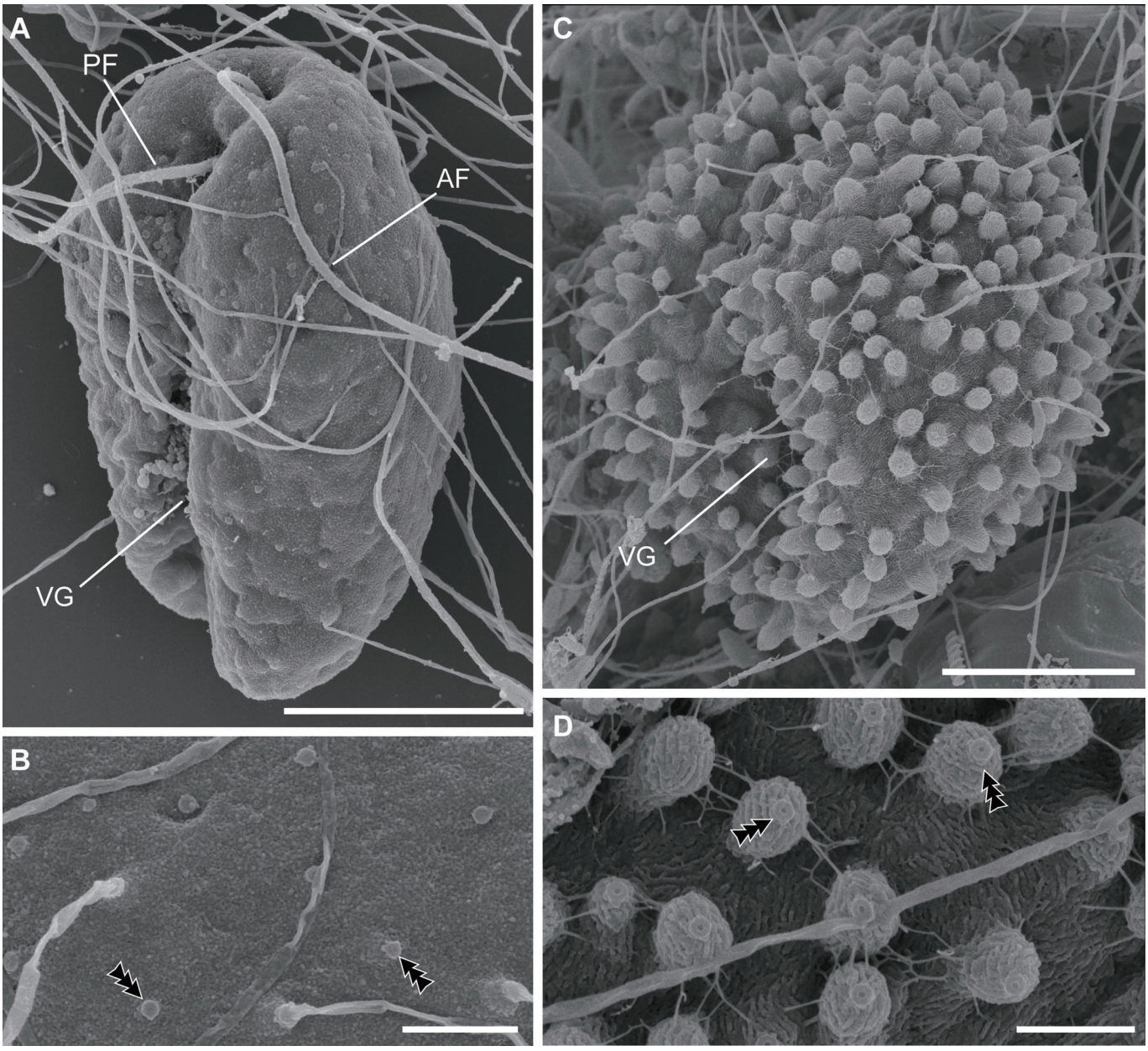

Figure 4

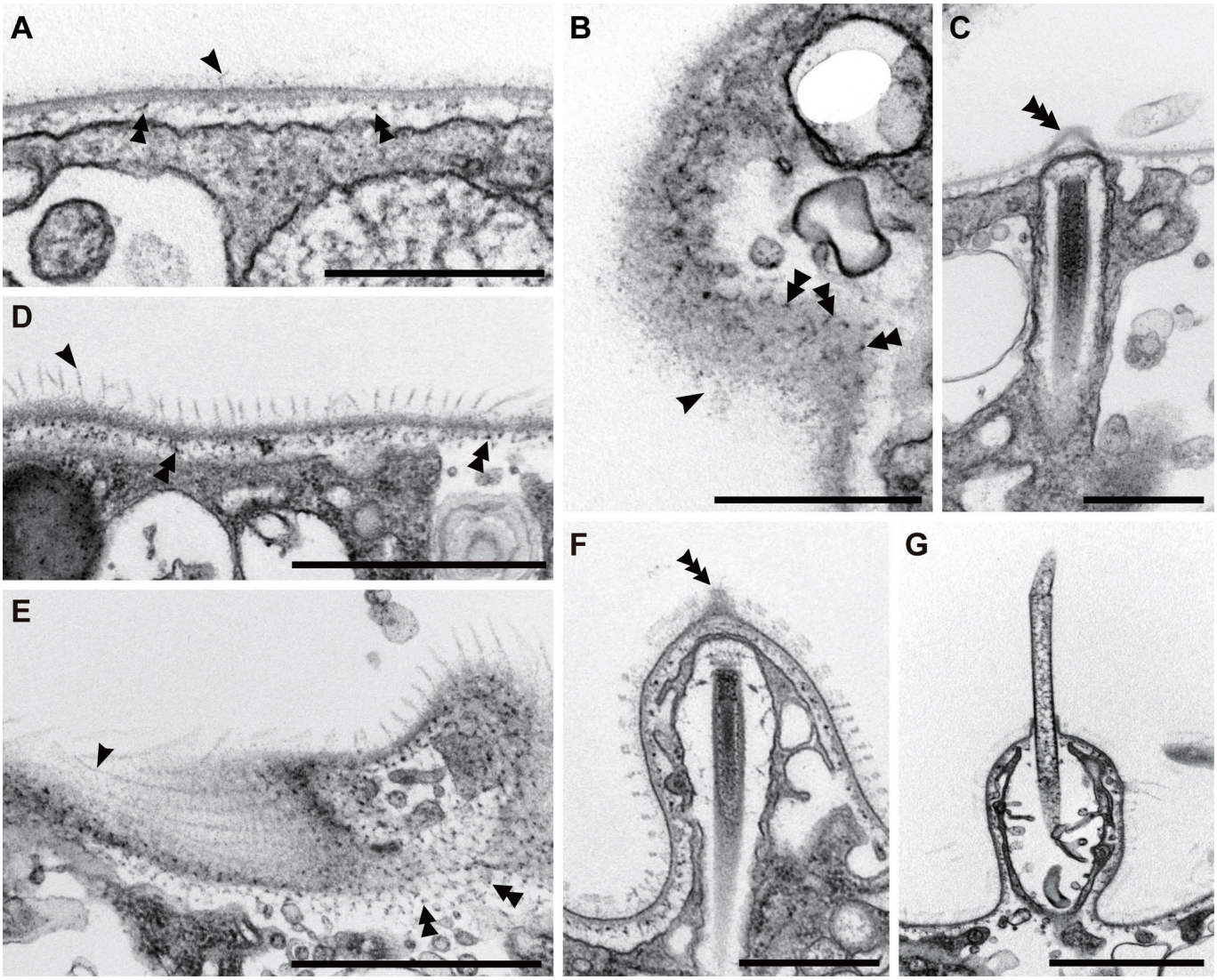

Figure 5

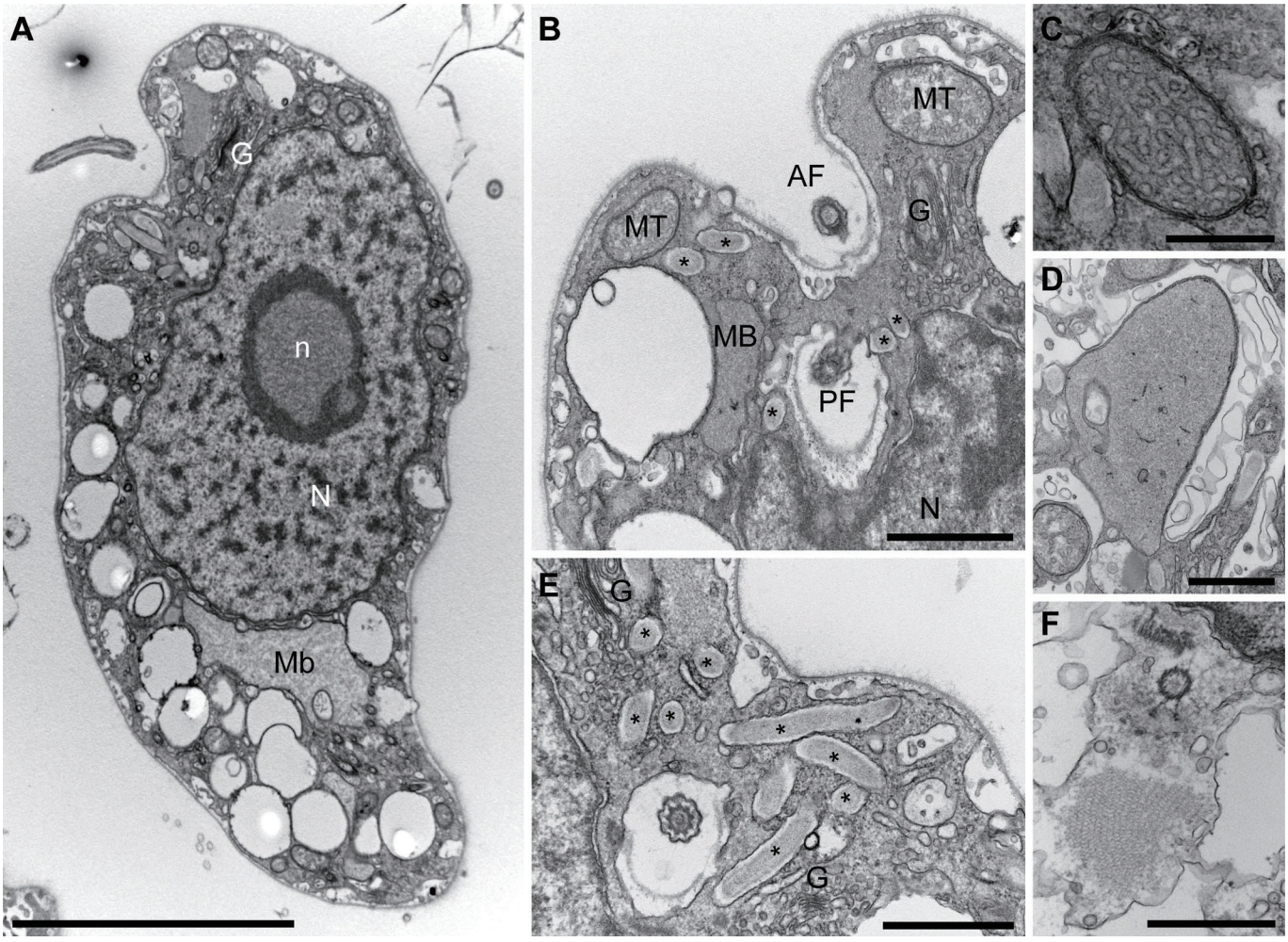

Figure 6

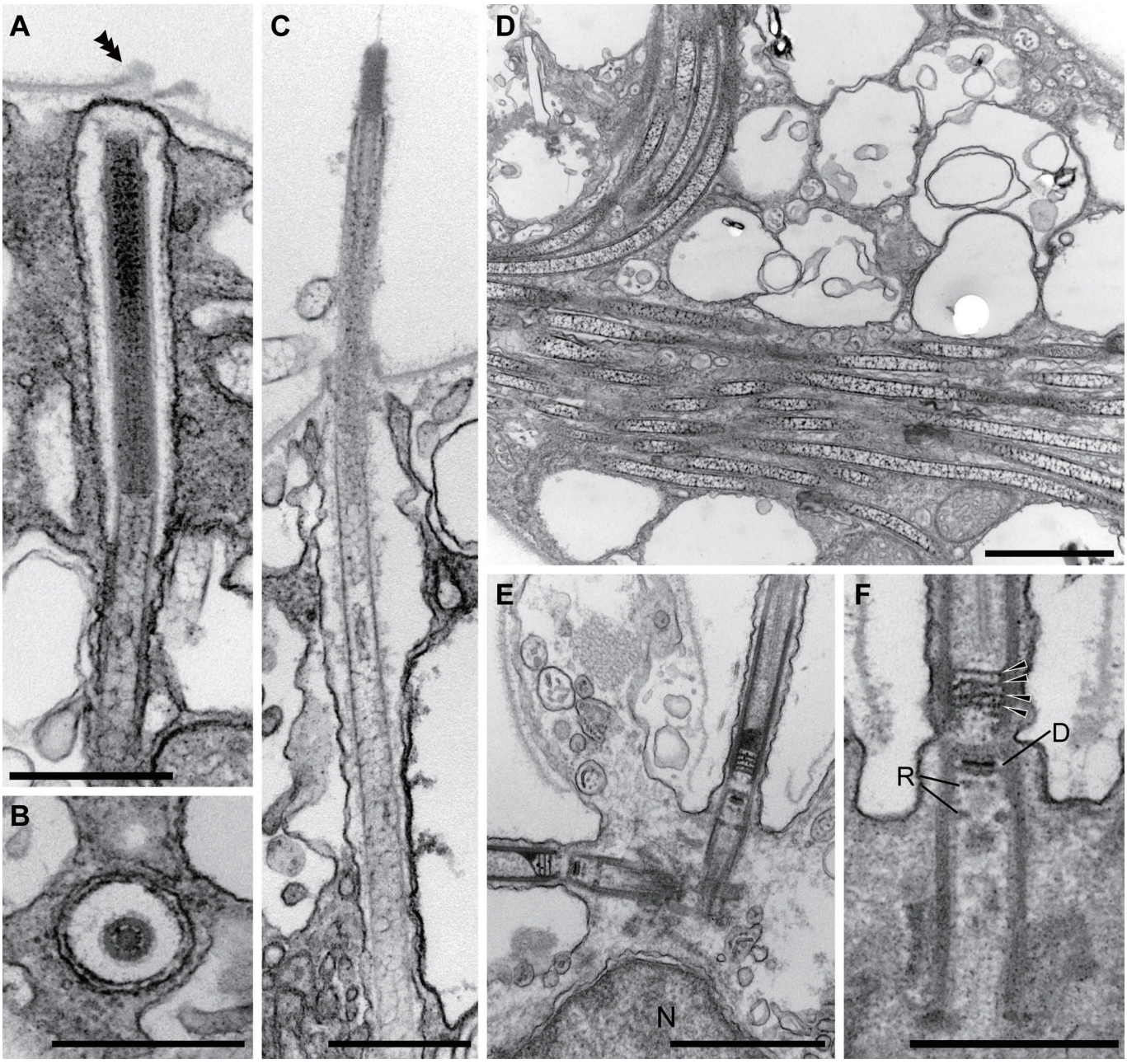

Figure 7

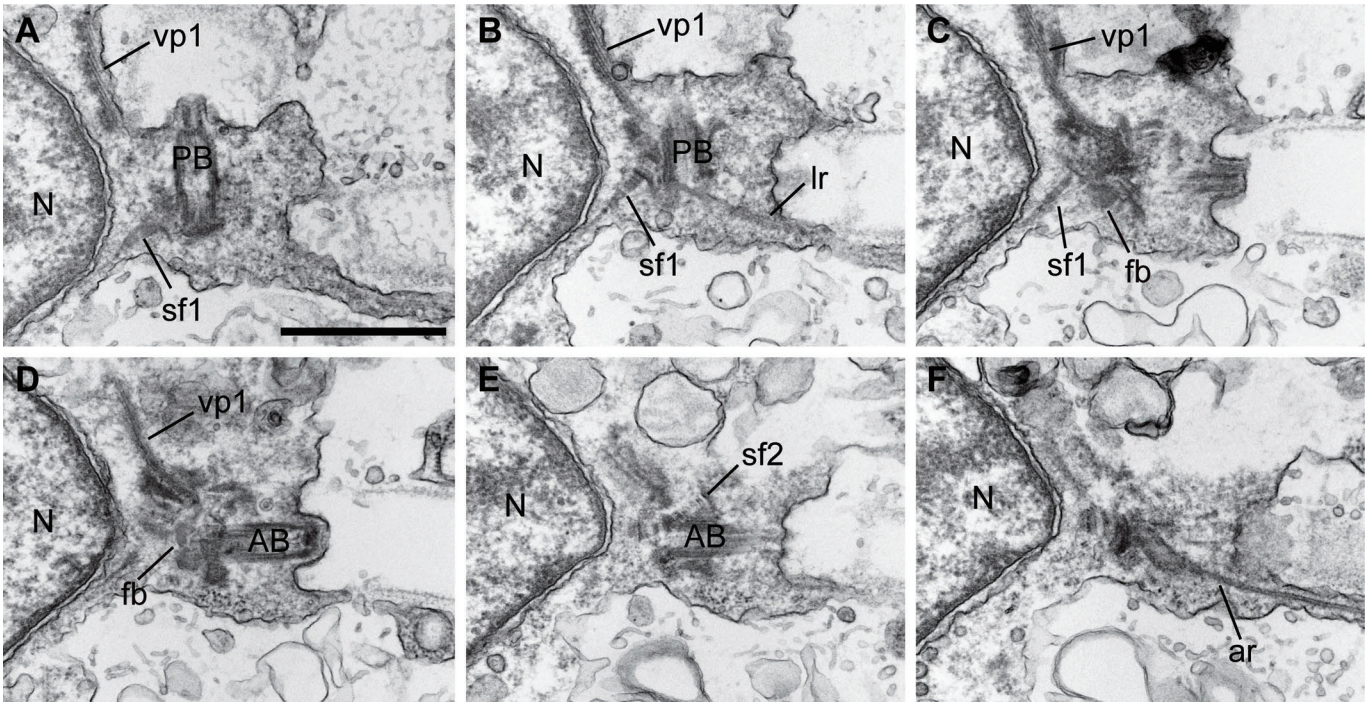
A
vp1
PB
N
sf1
B
vp1
N
PB
lr
sf1
C
vp1
N
sf1
fb
D
vp1
N
AB
fb
E
sf2
N
AB
F
N
ar

Figure 8

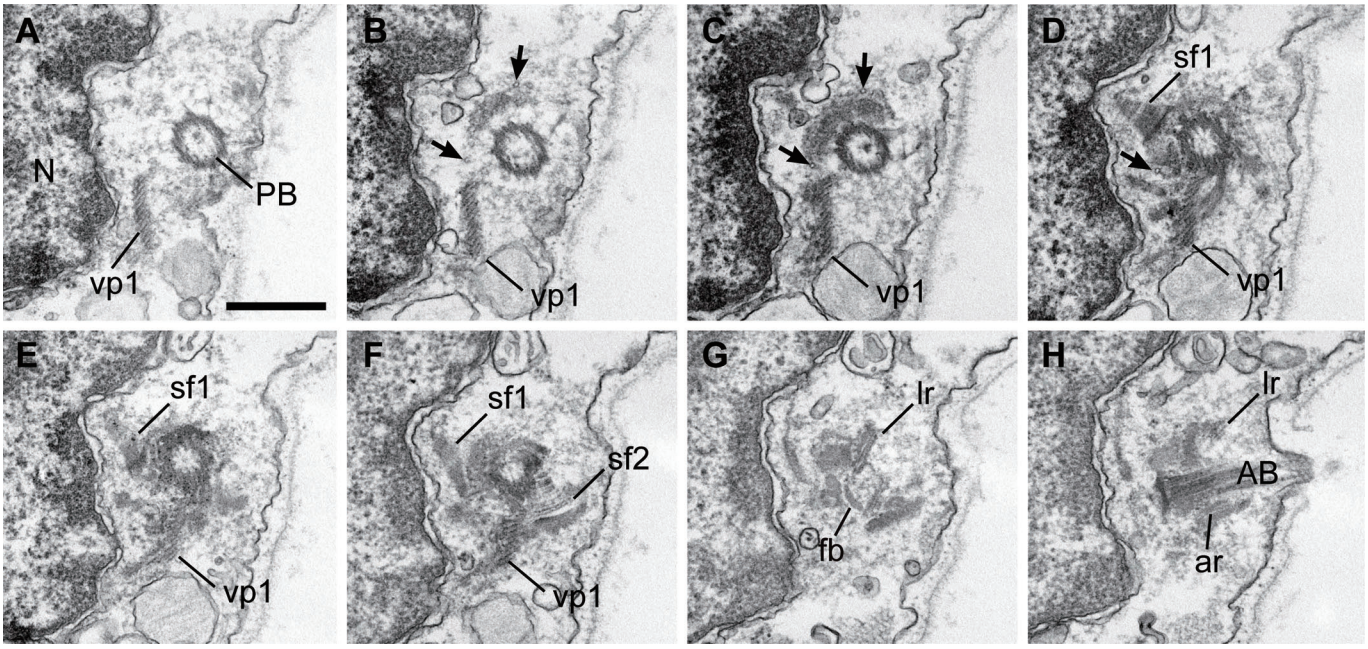
A
N
PB
vp1
B
vp1
C
vp1
D
sf1
vp1
E
sf1
vp1
F
sf1
sf2
vp1
G
lr
fb
H
lr
AB
ar

Figure 9

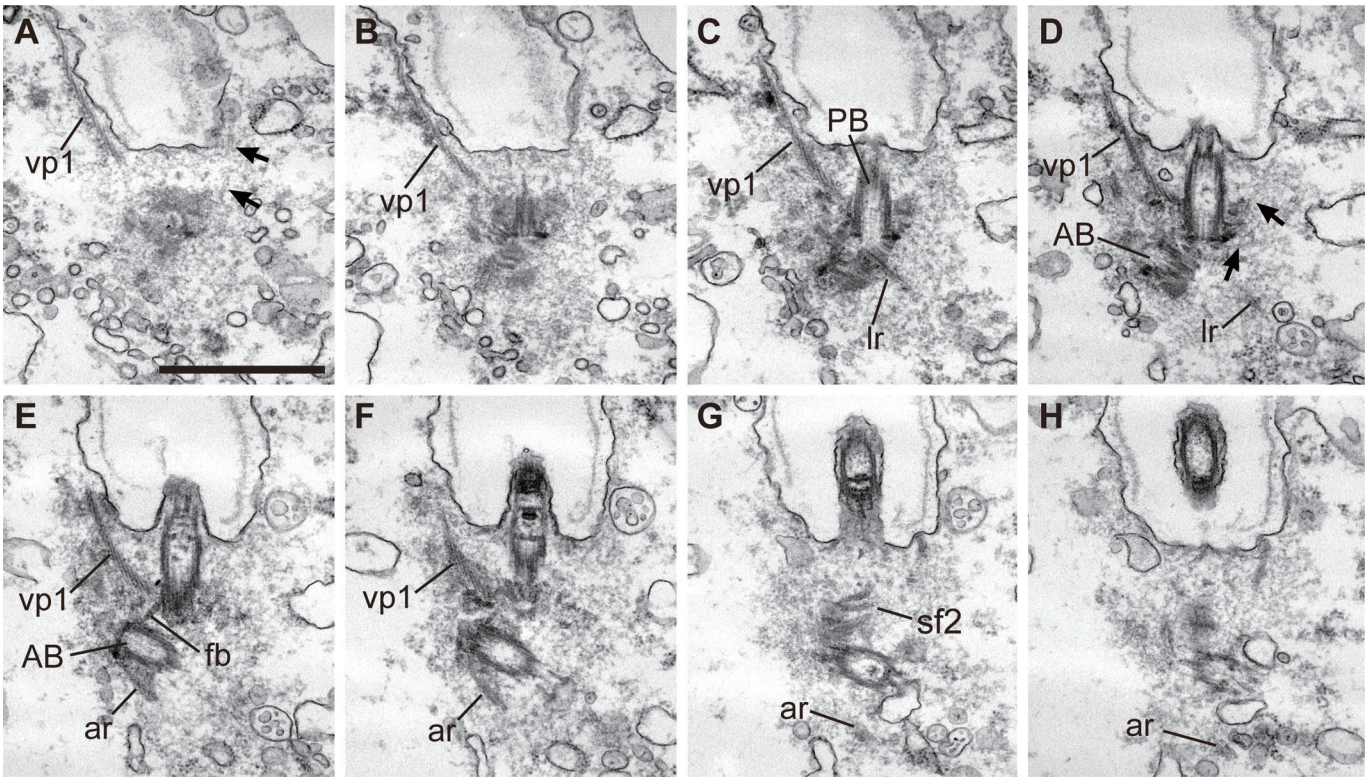

Figure 10

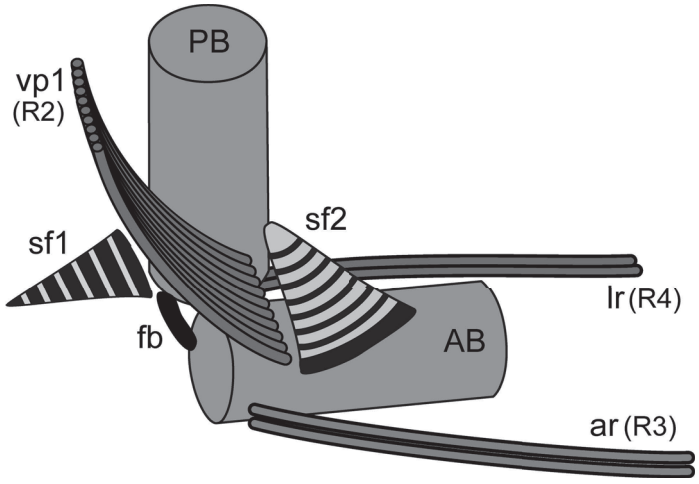

Figure 11

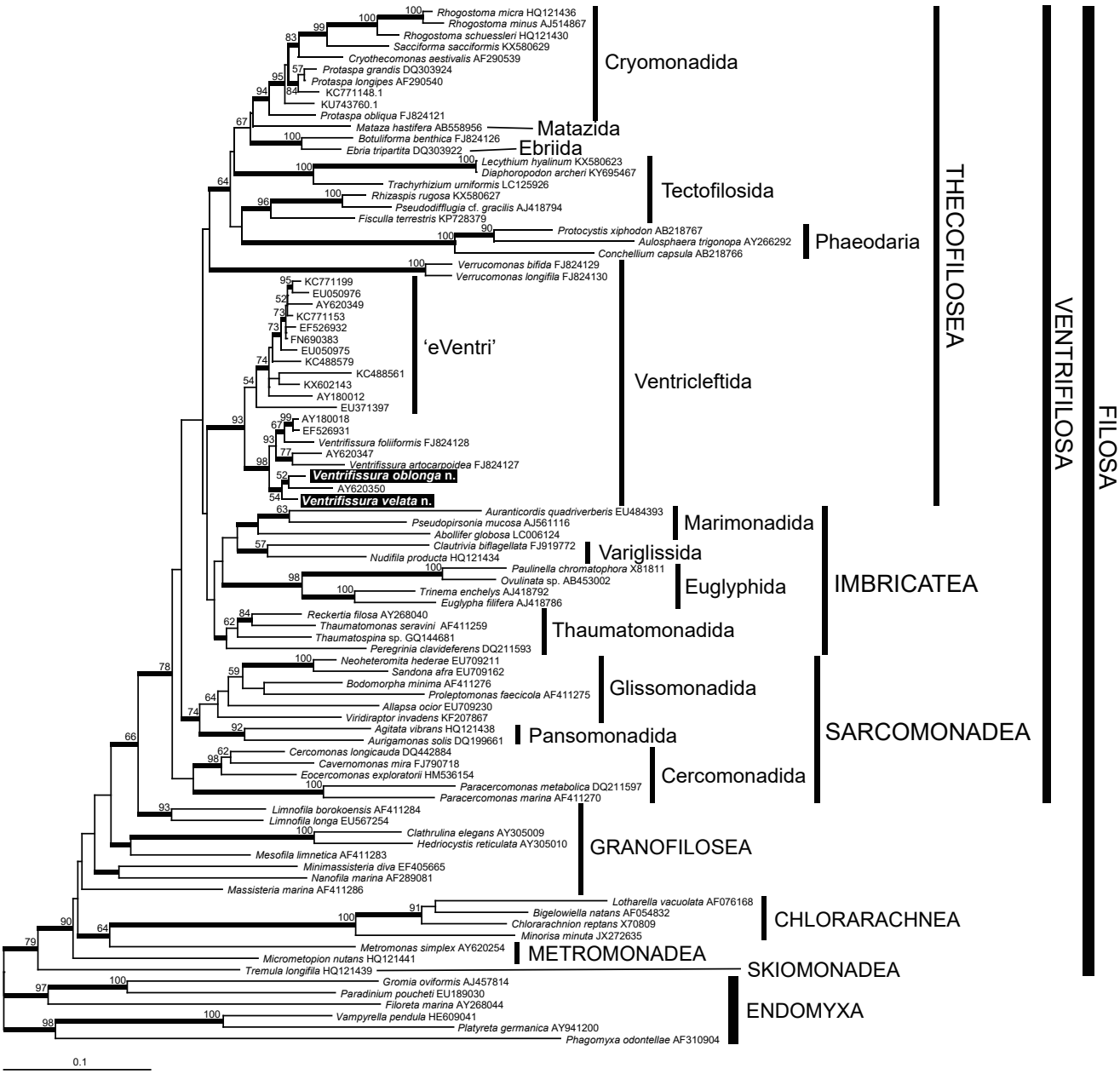
Rhogostoma micra HQ121436
Rhogostoma minus AJ514867
Rhogostoma schuessleri HQ121430
Sacciforma sacciformis KX580629
Cryothecomonas aestivalis AF290539
Protaspa grandis DQ303924
Protaspa longipes AF290540
KC771148.1
KU743760.1
Protaspa obliqua FJ824121
Mataza hastifera AB558956
Botuliforma benthica FJ824126
Ebria tripartita DQ303922
Lecythium hyalinum KX580623
Diaphoropodon archeri KY695467
Trachyrhizium urniformis LC125926
Rhizaspis rugosa KX580627
Pseudodiflugia cf. gracilis AJ418794
Fisculla terrestris KP728379
Protocystis xiphodon AB218767
Aulosphaera trigonopa AY266292
Conchellium capsula AB218766
Verrucomonas bifida FJ824129
Verrucomonas longifila FJ824130
KC771199
EU050976
AY620349
KC771153
EF526932
FN690383
EU050975
KC488579
KC488561
KX602143
AY180012
EU371397
AY180018
EF526931
Ventrifissura foliiformis FJ824128
AY620347
Ventrifissura artocarpoidea FJ824127
Ventrifissura oblonga n.
AY620350
Ventrifissura velata n.
Auranticordis quadriverberis EU484393
Pseudopirsonia mucosa AJ561116
Abollifer globosa LC006124
Clautrivia biflagellata FJ919772
Nudifila producta HQ121434
Paulinella chromatophora X81811
Ovulinata sp. AB453002
Trinema enchelys AJ418792
Euglypha filifera AJ418786
Reckertia filosa AY268040
Thaumatomonas seravini AF411259
Thaumatospina sp. GQ144681
Peregrinia clavideferens DQ211593
Neoheteromita hederae EU709211
Sandona afra EU709162
Bodomorpha minima AF411276
Proleptomonas faecicola AF411275
Allapsa ocior EU709230
Viridiraptor invadens KF207867
Agitata vibrans HQ121438
Aurigamonas solis DQ199661
Cercomonas longicauda DQ442884
Cavernomonas mira FJ790718
Eocercomonas exploratorii HM536154
Paracercomonas metabolica DQ211597
Paracercomonas marina AF411270
Limnofila borokoensis AF411284
Limnofila longa EU567254
Clathrulina elegans AY305009
Hedriocystis reticulata AY305010
Mesofila limnetica AF411283
Minimassisteria diva EF405665
Nanofila marina AF289081
Massisteria marina AF411286
Lotharella vacuolata AF076168
Bigelowiella natans AF054832
Chlorarachnion reptans X70809
Minorisa minuta JX272635
Metromonas simplex AY620254
Micrometopion nutans HQ121441
Tremula longifila HQ121439
Gromia oviformis AJ457814
Paradinium poucheti EU189030
Filoreta marina AY268044
Vampyrella pendula HE609041
Platyreta germanica AY941200
Phagomyxa odontellae AF310904
0.1
Cryomonadida
Matazida
Ebriida
Tectofilosida
Phaeodaria
THECOFILOSEA
'eVentri'
Ventricleftida
Marimonadida
Variglissida
Euglyphida
Thaumatomonadida
IMBRICATEA
Glissomonadida
Pansomonadida
Cercomonadida
SARCOMONADEA
VENTRIFILOSA
GRANOFILOSEA
CHLORARACHNEA
METROMONADEA
SKIOMONADEA
ENDOMYXA
FILOSA